Fault-Tolerant Control of Half-Centralized Open-End Winding Motor Drive System Considering Open-Circuit Faults

Weijie Tian, Wei Wang, *Senior Member, IEEE*, Wei Hua, *Senior Member, IEEE*, and Ming Cheng, *Fellow, IEEE*

***Abstract*—In this article, a fault-tolerant control method is designed for half-centralized open-end winding (HCOW) motor drive system with open-circuit fault. In the HCOW drive system, each mover can output fluctuated thrust and the system thrust should keep constant. This will provide additional degree of thrust freedom, which may lead to less system copper loss or higher torque (thrust) output capacity. The proposed fault-tolerant control method includes two fault current distributors and one voltage distributor. The fault current distributor I is designed for the common-leg fault based on the Lagrange loss minimization principle. The fault current distributor II is designed for the independent-leg fault based on the fundamental frequency phase loss minimization principle. The voltage distributor is designed to distribute the voltage demand into remaining inverter legs. The system copper losses and the thrust output capacity of the different methods are analyzed. Compared with the conventional method, the proposed tolerant method can reduce the system copper loss and increase the thrust output capacity. Finally, the proposed fault-tolerant control method has been verified by experimental results.**

***Index Terms*—Fault tolerance, open-circuit fault (OCF), open-end winding motor drive system.**

I. Introduction

PERMANENT-MAGNET motors have been applied in many fields due to the high efficiency and high-power density [1], [2], [3]. With the merits of wide speed range operations, excellent fault-tolerant ability, and multilevel modulation, open-end winding drive systems have been studied by lots of researchers [4], [5], [6].

Usually, an open-end winding permanent-magnet motor is supplied by two voltage source inverters (VSIs), which will bring some drawbacks, such as more expensive hardware cost and higher failure possibility. The abovementioned drawbacks will be more serious for multimotor drive system. In [7], a half-centralized open-end winding (HCOW) motor drive system is proposed, which not only retains the advantages of conventional open-end winding drive system, but also reduces the number of power switches. In [7], a collaborative control method is applied to realize the high performance of HCOW drive system and the voltage distributor can maximize the dc voltage utilization. In [8], two unified maximum voltage utilization control methods are proposed and compared to expand the speed range of HCOW drive system. In [9], two model predictive voltage control methods are designed from the perceptive of phase for HCOW drive system.

According to [10], the open-circuit fault (OCF) is one of the common faults in the drive system and open-circuit accounts for up to 38%. The control performance and efficiency of drive system will degrade. Even in some cases, it will result in serious damage. Up to now, many fault-tolerant control methods have been proposed to cope with OCFs of motor drive systems [11], [12], [13], [14], [15], [16], [17], [18], [19], [20], [21], [22]. Conventional drive topology can realize the fault tolerance of OCF [11], [12], [13]. However, for the fault tolerance of three-phase motor drive system, special drive topologies should be applied, such as open-end winding topology [14], [15], [16], [17] and four-leg topology [18], [19], [20], [21], [22]. For the open-end winding topology, a new coordinate transformation matrix is designed to realize the fault tolerance of OCF [14]. This method can decouple the voltage expression and suppress the torque ripple. In [15], a fault-tolerant predictive controller is proposed for the open-end winding topology with OCF, which can be applied in both pre and postfault conditions. In [16], the second-time OCF is processed by bridge arm sharing strategy and the reliability of drive system can be further enhanced. In [17], an optimal real-time fault-tolerant control method is designed to reduce the system copper loss in the open-end winding topology with OCF. In [18], a novel transformation matrix is designed to transform the dq-axis demand into remaining phase demand under OCF condition. In [19], a new reference frame transformation is proposed for OCF. This method can be applied in both $i_d = 0$ mode and $i_d \neq 0$ mode. In [20], an optimized fault-tolerant control method is designed with the consideration of system copper loss minimization and magnetomotive force constant. In [21], two resonant controllers are applied for the fault tolerance of OCF. This method can adaptively suppress

Manuscript received 12 June 2023; accepted 5 August 2023. Date of publication 9 August 2023; date of current version 22 September 2023. This work was supported in part by the Jiangsu Natural Science Foundation of China under Grant BK20200066, in part by the National Natural Science Foundation of China under Grant 51977036 and Grant 51991384, and in part by the Postgraduate Research & Practice Innovation Program of Jiangsu Province under Grant KYCX22_0259. Recommended for publication by Associate Editor B. Mirafzal. *(Corresponding author: Wei Wang.)*

The authors are with the School of Electrical Engineering, Southeast University, Nanjing 210096, China (e-mail: tianweijie@seu.edu.cn; wangwei1986@seu.edu.cn; huawei1978@seu.edu.cn; mcheng@seu.edu.cn).

Color versions of one or more figures in this article are available at https://doi.org/10.1109/TPEL.2023.3303433.

Digital Object Identifier 10.1109/TPEL.2023.3303433

second harmonic in the torque ripple. In [22], the third harmonic back electromotive force (EMF) is taken into account, and the second and fourth harmonic torque can be suppressed. In [23], the fault-tolerant operation of the motor with Δ-connected circuits is achieved by the constant volts-per-hertz control. In [24], a fault-tolerant control was proposed for the open-end winding induction motor drive, in which a multilevel inverter was employed. These literatures [23] and [24] are mainly designed for single three-phase motors, while the HCOW drive system contains several three-phase motors. In addition, multiphase motors have stronger fault-tolerant capacity [25], [26], [27], [28], [29]. Based on the redundancy communication and redundancy bridge arm [25], [26], two fault-tolerant control methods are, respectively, designed for the dual three-phase motor system with Y-connected circuit. However, the neutral point is opened in the HCOW systems. In [27], the current vector fault-tolerant method was applied for the dual three-phase open-end winding motor system, and the two sets of three-phase windings must always remain same phase angles. However, the phase angles of the motors in the HCOW drive system may be different. Unfortunately, to the best of authors' knowledge, no existing literatures can be directly applied for the fault tolerance of the HCOW drive system.

To improve the reliability of the HCOW drive system, a fault-tolerant control method is proposed in this article to cope with the OCF of the HCOW drive system. The main contribution of this article is to achieve the fault-tolerant control of the HCOW drive system, while the copper losses and thrust output capacity are optimized according to different targets. Compared with the conventional method, which extends from the open-end winding fault-tolerant system, the proposed method can reduce system copper losses and increase the thrust output capacity. The rest of the article is organized as follows. The studied HCOW drive system is introduced in Section II. The proposed fault-tolerant control method is proposed in Section III. The conventional fault-tolerant control method is shown in Section IV. The performance is analyzed in Section V. Some experiments are carried out to verify the effectiveness of the proposed fault-tolerant control method in Section VI. Finally, Section VII concludes this article.

II. HCOW Drive System Description

The HCOW drive system has been proposed in the previous articles [7], which consists of three VSIs and two movers. One side of each mover is connected to an independent VSI and the other sides of all motors are connected to a common VSI. Compared with the open-winding drive system, the HCOW drive system can be applied to reduce the power switches.

The voltage equation of each mover in the HCOW drive system is the same as the conventional forms, which can be described as

$$\begin{bmatrix} u_{ay} \\ u_{by} \\ u_{cy} \end{bmatrix} = R_{sy} \begin{bmatrix} i_{ay} \\ i_{by} \\ i_{cy} \end{bmatrix} + \begin{bmatrix} L & M & M \\ M & L & M \\ M & M & L \end{bmatrix} \begin{bmatrix} i_{ay} \\ i_{by} \\ i_{cy} \end{bmatrix} + \begin{bmatrix} e_{ay} \\ e_{by} \\ e_{cy} \end{bmatrix} \quad (1)$$

where u_{ay}, u_{by}, and u_{cy} are phase voltages of mover y, respectively; i_{ay}, i_{by}, and i_{cy} are current of mover y, respectively; L and M are the phase self-inductance and mutual inductance, respectively; R_{sy} is the phase resistance; e represents back EMF; and the subscripts y indicates mover y ($y = 1$ or 2). The HCOW drive system thrust is superimposed by all movers. The thrust F can be deduced as

$$F = \frac{e_{a1}i_{a1} + e_{b1}i_{b1} + e_{c1}i_{c1} + e_{a2}i_{a2} + e_{b2}i_{b2} + e_{c2}i_{c2}}{v} \quad (2)$$

where v is the system speed, $v = \omega_e \tau_s/2\pi$. ω_e is the equivalent electrical angular velocity; and τ_s is the double pole pitch. These EMFs are described as

$$\begin{cases} e_{a1} = -E\sin(\theta_1), & e_{a2} = -E\sin(\theta_1 + \Delta\theta) \\ e_{b1} = -E\sin(\theta_1 - 2\pi/3), & e_{b2} = -E\sin(\theta_1 - 2\pi/3 + \Delta\theta) \\ e_{c1} = -E\sin(\theta_1 + 2\pi/3), & e_{c2} = -E\sin(\theta_1 + 2\pi/3 + \Delta\theta) \end{cases} \quad (3)$$

where E is the EMF amplitude, $E = \omega_e\psi_f$; ψ_f is the fundamental amplitudes of the permanent-magnet flux linkage; $\Delta\theta$ is the primary position difference, $\Delta\theta = \theta_2 - \theta_1$; and θ_1 and θ_2 are the primary positions of two movers. Specially, the permanent-magnet flux linkage can be measured offline. The measurement method can be summarized as follow: 1) use another motor drive measured motor at a constant speed and measure the EMF at both ends of the phase winding; 2) extract the amplitude E of the EMF and calculate $\omega_e = 2\pi\nu/\tau_s$; and 3) calculate $\psi_f = E/\omega_e$.

The voltage demands are modulated by three VSIs

$$\begin{cases} u_{ay} = (\delta_{ay} - \delta_{ap})\, u_{\mathrm{dc}} \\ u_{by} = (\delta_{by} - \delta_{bp})\, u_{\mathrm{dc}} \\ u_{cy} = (\delta_{cy} - \delta_{cp})\, u_{\mathrm{dc}} \end{cases} \quad (4)$$

where u_{dc} is dc voltage; δ_{ay}, δ_{by}, and δ_{cy} are leg duty ratio of independent VSI y. δ_{ap} is leg duty ratio of common VSI p.

When the OCF occurs in one VSI, the mover connected to this VSI is named fault mover. The studied HCOW–PPMLM drive system with OCF is shown in Fig. 1. Two types of OCFs are taken into account. The first one is the independent-leg fault as shown in Fig. 1(a), in which the OCF occurs in one leg of the independent VSI. In the independent-leg fault condition, only five phase windings can be used. Hence, the fault tolerance of the independent-leg fault focuses more on improving the thrust output capability. The second one is the common-leg fault as shown in Fig. 1(b), in which the OCF occurs in one leg of the common VSI. In the common-leg fault condition, there are still six phase windings available for use. Hence, the fault tolerance of the common-leg fault focuses more on reducing system losses. In order to simplify the analysis, the independent-leg fault occurs in leg-a2 and the common-leg fault occurs in leg-aP.

III. Proposed Fault-Tolerant Control Method

In this section, the fault-tolerant control method is proposed for the HCOW drive system, which includes one healthy current distributor, one current regulator, two fault current distributors, and one voltage distributor. The control diagram is shown in Fig. 2. The fault current distributors and the voltage distributor

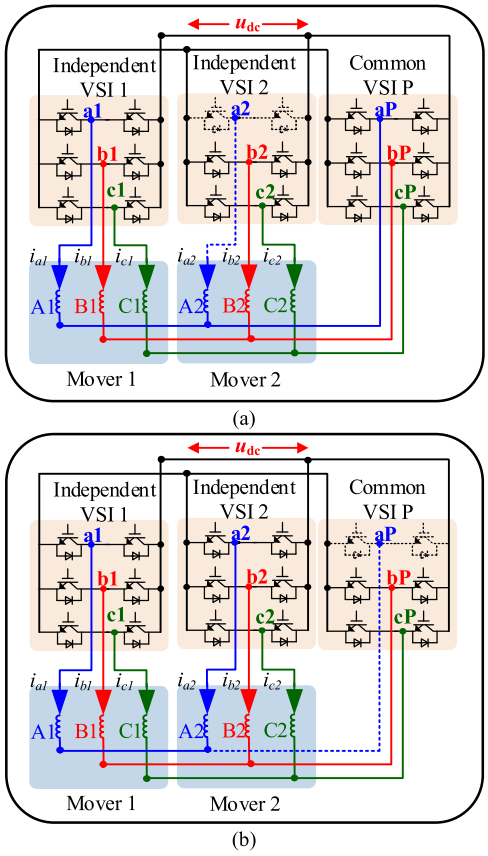

Fig. 1. Studied HCOW drive system with open-circuit fault. (a) Independent-leg fault. (b) Common-leg fault.

are explained in detail. On the other hand, the healthy current distributor and the current regulator will not be discussed in this article since they have been proposed in the previous article [7].

For the common-leg fault, two additional degrees of freedom can be released as follows:

1) The total thrust of two movers should keep constant. This means that two movers only need to satisfy one thrust (power) constraint. In conventional method, two movers need to output constant thrust separately and satisfy two thrust (power) constraints.
2) The sum of fault phase currents should be zero. This means fault phase current only needs to satisfy one current constraint. In conventional method, two phase currents both need to be zero and satisfy two current constraints. For the independent-leg fault, one additional degrees of freedom can be released, which is same as above point 1.

A. Fault Current Distributor I

The fault current distributor I is designed for the common-leg fault based on the Lagrange loss minimization principle.

Based on the thrust constraint in HCOW drive system, these phase currents satisfy (2). The OCF will bring additional current constraint as

$$ki_{a1} + i_{a2} = 0 \tag{5}$$

where k is the fault type flag (0 represents the independent-leg fault and 1 represents the common-leg fault).

Based on (2) and (5), the Lagrange function can be established as

$$\begin{aligned} J = {} & i_{a1}^2 + i_{b1}^2 + i_{c1}^2 + i_{a2}^2 + i_{b2}^2 + i_{c2}^2 + \lambda_2[ki_{a1} + i_{a2}] \\ & + \lambda_1 \left[\mathrm{e}_{a1}i_{a1} + \mathrm{e}_{b1}i_{b1} + \mathrm{e}_{c1}i_{c1} + \mathrm{e}_{a2}i_{a2}\right. \\ & \left. + \mathrm{e}_{b2}i_{b2} + \mathrm{e}_{c2}i_{c2} - \mathrm{Fv}\right] \end{aligned} \tag{6}$$

where λ_1 and λ_2 are the Lagrange coefficient.

The partial differential can be obtained as

$$\begin{cases} \dfrac{\partial J}{\partial i_{a1}} = 2i_{a1} + \mathrm{e}_{a1}\lambda_1 + k\lambda_2 = 0, & \dfrac{\partial J}{\partial i_{a2}} = 2i_{a2} + \mathrm{e}_{a2}\lambda_1 + \lambda_2 = 0 \\ \dfrac{\partial J}{\partial i_{b1}} = 2i_{b1} + \mathrm{e}_{b1}\lambda_1 = 0, & \dfrac{\partial J}{\partial i_{b2}} = 2i_{b2} + \mathrm{e}_{b2}\lambda_1 = 0 \\ \dfrac{\partial J}{\partial i_{c1}} = 2i_{c1} + \mathrm{e}_{c1}\lambda_1 = 0, & \dfrac{\partial J}{\partial i_{c2}} = 2i_{c2} + \mathrm{e}_{c2}\lambda_1 = 0 \\ \dfrac{\partial J}{\partial \lambda_1} = \mathrm{e}_{a1}i_{a1} + \mathrm{e}_{b1}i_{b1} + \mathrm{e}_{c1}i_{c1} + \mathrm{e}_{a2}i_{a2} + \mathrm{e}_{b2}i_{b2} + \mathrm{e}_{c2}i_{c2} - \mathrm{Fv} = 0 \\ \dfrac{\partial J}{\partial \lambda_2} = ki_{a1} + i_{a2} = 0 \end{cases} \tag{7}$$

The phase current can be calculated by

$$\begin{cases} i_{a1} = \dfrac{Fv\left[k\sin(\theta_1 + \Delta\theta) - \sin(\theta_1)\right]}{EQ}, \\ i_{a2} = -\dfrac{kFv\left[k\sin\left(\theta_1 + \Delta\theta\right) - \sin(\theta_1)\right]}{EQ} \\ i_{b1} = -\dfrac{Fv(1+k^2)\sin\left(\theta_1 - 120\right)}{EQ}, \\ i_{b2} = -\dfrac{Fv(1+k^2)\sin\left(\theta_1 + \Delta\theta - 120\right)}{EQ} \\ i_{c1} = -\dfrac{Fv(1+k^2)\sin\left(\theta_1 + 120\right)}{EQ}, \\ i_{c2} = -\dfrac{Fv(1+k^2)\sin\left(\theta_1 + \Delta\theta + 120\right)}{EQ} \end{cases} \tag{8}$$

where

$$Q = 3(1+k^2) - \left[\sin(\theta + \Delta\theta) + k\sin(\theta)\right]^2.$$

For different movers, the $dq0$-axis synchronous current can be calculated by Park transformation

$$\begin{bmatrix} i_{dy}^* \\ i_{qy}^* \\ i_{0y}^* \end{bmatrix} = \frac{2}{3}\begin{bmatrix} \cos(\theta_y) & \cos(\theta_y - 2\pi/3) & \cos(\theta_y + 2\pi/3) \\ -\sin(\theta_y) & -\sin(\theta_y - 2\pi/3) & -\sin(\theta_y + 2\pi/3) \\ 1/2 & 1/2 & 1/2 \end{bmatrix} \times \begin{bmatrix} i_{ay}^* \\ i_{by}^* \\ i_{cy}^* \end{bmatrix} \tag{9}$$

where i_{ay}^*, i_{by}^* and i_{cy}^* are the reference phase current of mover y; i_{dy}^*, i_{qy}^* and i_{0y}^* are the reference $dq0$-axis current of mover y; and θ_y is the electrical angle of mover y.

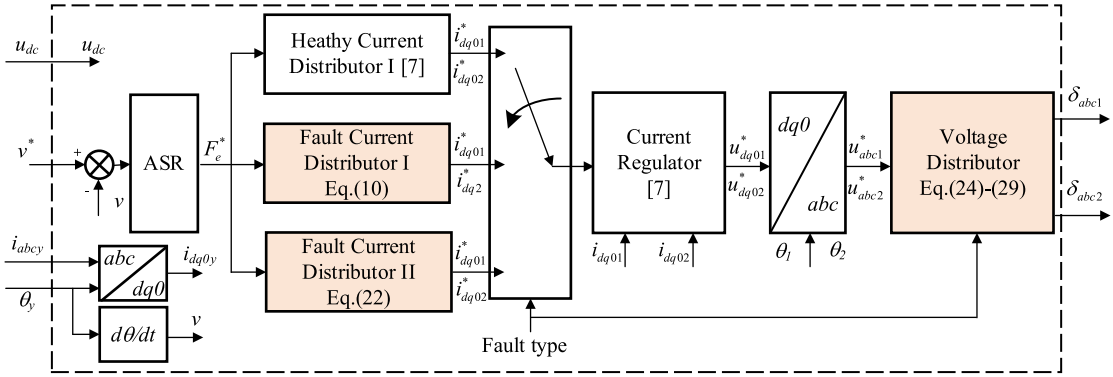

Fig. 2. Proposed fault-tolerant control method.

For the common-leg fault, the reference $dq0$-axis currents can be deduced by bringing $k = 1$ and (8) into (9). Then, the fault current I can be described as

$$\begin{cases} i_{d1}^* = (I_m/3Q)\left[2\cos(\Delta\theta/2)\sin(2\theta_1+\Delta\theta/2)+\sin(\Delta\theta)\right] \\ i_{q1}^* = (I_m/3Q)\left[5+2\cos(\Delta\theta/2)\cos(2\theta_1+\Delta\theta/2)\right. \\ \qquad\qquad \left.-\cos(\Delta\theta)\right] \\ i_{01}^* = (I_m/3Q)[\sin(\theta_1+\Delta\theta)+\sin(\theta_1)] \\ i_{d2}^* = (I_m/3Q)\left[2\cos(\Delta\theta/2)\sin(2\theta_1+3\Delta\theta/2)-\sin(\Delta\theta)\right] \\ i_{q1}^* = (I_m/3Q)\left[5+2\cos(\Delta\theta/2)\cos(2\theta_1+3\Delta\theta/2)\right. \\ \qquad\qquad \left.-\cos(\Delta\theta)\right] \\ i_{02}^* = (I_m/3Q)\left[\sin(\theta_1)+\sin(\theta_1+\Delta\theta)\right] \end{cases} \tag{10}$$

where I_m can be calculated as

$$I_m = \tau_s F/(2\pi\psi_f). \tag{11}$$

B. Fault Current Distributor II

In order to enhance the thrust output capacity for the independent-leg fault, the remaining phase currents are deduced according to the fundamental frequency loss minimization principle, in which all phase currents are distributed as

$$\begin{cases} i_{a1} = [X_{a1}\cos(\theta_1)+Y_{a1}\sin(\theta_1)]\,I_m \\ i_{a2} = [X_{a2}\cos(\theta_1+\Delta\theta)+Y_{a2}\sin(\theta_1+\Delta\theta)]\,I_m \\ i_{b1} = [X_{b1}\cos(\theta_1)+Y_{b1}\sin(\theta_1)]\,I_m \\ i_{b2} = [X_{b2}\cos(\theta_1+\Delta\theta)+Y_{b2}\sin(\theta_1+\Delta\theta)]\,I_m \\ i_{c1} = [X_{c1}\cos(\theta_1)+Y_{c1}\sin(\theta_1)]\,I_m \\ i_{c2} = [X_{c2}\cos(\theta_1+\Delta\theta)+Y_{c2}\sin(\theta_1+\Delta\theta)]\,I_m \end{cases} \tag{12}$$

where X_x and Y_x are unknown coefficient of phase x. The subscript x indicates different phases ($x = a1, a2, \ldots, c2$).

Taking (12) into (2) gives the current constraint as

$$\frac{Fv}{\mathrm{EI}_m} = L_1 + L_2\cos(2\theta_1) + L_3\sin(2\theta_1) \tag{13}$$

where

$$\begin{cases} L_1 = 0.25(-2Y_{a1}+\sqrt{3}X_{b1}+Y_{b1}-\sqrt{3}X_{c1}+Y_{c1} \\ \qquad -2Y_{a2}+\sqrt{3}X_{b2}+Y_{b2}-\sqrt{3}X_{c2}+Y_{c2}) \\ L_2 = -X_{a1}-X_{b1}\cos(2\pi/3)+Y_{b1}\sin(2\pi/3) \\ \qquad -X_{c1}\cos(2\pi/3)-Y_{c1}\sin(2\pi/3)-X_{a2}\cos(2\Delta\theta) \\ \qquad -Y_{a2}\sin(2\Delta\theta)-X_{b2}\cos(2\Delta\theta-2\pi/3) \\ \qquad -Y_{b2}\sin(2\Delta\theta-2\pi/3)-X_{c2}\cos(2\Delta\theta+2\pi/3) \\ \qquad -Y_{c2}\sin(2\Delta\theta+2\pi/3) \\ L_3 = Y_{a1}+X_{b1}\sin(2\pi/3)+Y_{b1}\cos(2\pi/3)-X_{c1}\sin(2\pi/3) \\ \qquad +Y_{c1}\cos(2\pi/3)-X_{a2}\sin(2\Delta\theta)+Y_{a2}\cos(2\Delta\theta) \\ \qquad -X_{b2}\sin(2\Delta\theta-2\pi/3)+Y_{b2}\cos(2\Delta\theta-2\pi/3) \\ \qquad -X_{c2}\sin(2\Delta\theta+2\pi/3)+Y_{c2}\cos(2\Delta\theta+2\pi/3) \end{cases}$$

In order to eliminate the thrust ripples, L_1, L_2, and L_3 should satisfy

$$L_1 = 1, L_2 = L_3 = 0. \tag{14}$$

Taking (12) into (5) gives the current constraint as

$$\begin{cases} kX_{a1}+X_{a2}\cos(\Delta\theta)+Y_{a2}\sin(\Delta\theta) = 0 \\ kY_{a1}-X_{a2}\sin(\Delta\theta)+Y_{a2}\cos(\Delta\theta) = 0. \end{cases} \tag{15}$$

The average phase copper loss P_x can be calculated by

$$\mathrm{P}_x = \frac{1}{\mathrm{T}}\int_0^T R_x i_x^2 dt = \frac{1}{2\pi}\int_0^{2\pi} R_x i_x^2 d\theta \tag{16}$$

where R_x is the phase resistance. The maximum phase loss P_{pm} is defined as

$$P_{\mathrm{pm}} = \max(P_{a1}, P_{b1}, P_{c1}, P_{a2}, P_{b2}, P_{c2}). \tag{17}$$

In order to simplify the analysis, it is assumed that the reference thrust is implemented in healthy condition. As a result, the equivalent thrust current I_h can be calculated by

$$I_h = \frac{\tau_s F}{6\pi\psi_f} = \frac{I_m}{3}. \tag{18}$$

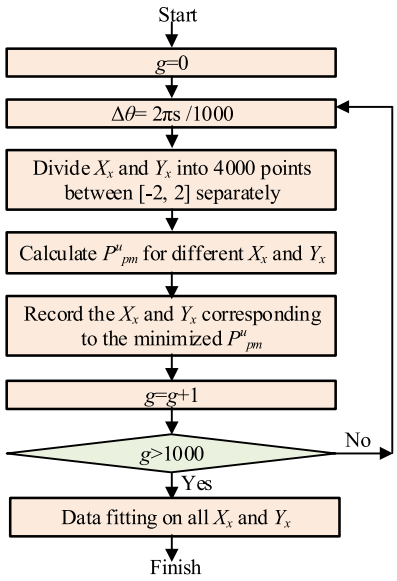

Fig. 3. Solution process of the optimization equation.

It should be emphasized that the reference thrust may be actually implemented in the independent-leg fault or the common-leg fault.

In order to eliminate the effect of current amplitude and thrust demand, average phase copper loss P_x is standardized based on the loss under healthy condition. $0.5R_xI_h^2$ is set as the base value. After standardization, (16) and (17) can be represented as

$$\begin{cases} \mathrm{P}_x^u = \frac{1}{2\pi}\int_0^{2\pi} \frac{R_x i_x^2}{0.5R_xI_h^2}d\theta = \frac{9}{\pi}\int_0^{2\pi}(\frac{i_x}{I_m})^2 d\theta \\ P_{pm}^u = \max(P_{a1}^u, P_{b1}^u, P_{c1}^u, P_{a2}^u, P_{b2}^u, P_{c2}^u) \end{cases} \tag{19}$$

where the superscript u indicates standardization.

Based on the minimized maximum phase loss principle, the optimization goal p_{MPL} can be established as

$$p_{\mathrm{MPL}} = \min\left[\max\left(P_{a1}^u, P_{b1}^u, P_{c1}^u, P_{a2}^u, P_{b2}^u, P_{c2}^u\right)\right]. \tag{20}$$

Combing the current constraint with the optimization goal (20), an optimization equation can be established. Then, the coefficients (X_x and Y_x) can be deduced offline by the enumeration method as shown in Fig. 3. These steps can be elaborated as follows:

1) Initialize $g = 0$.
2) Calculate $\Delta\theta = 2\pi s/1000$.
3) Divide X_x and Y_x into 4000 points between $[-2, 2]$ separately.
4) Substitute the different combinations of X_x and Y_x into formulas (12) and (19) to calculate $P^u{}_{\mathrm{pm}}$.
5) Record the X_x and Y_x corresponding to the minimized $P^u{}_{\mathrm{pm}}$.
6) Calculate $g = g + 1$.
7) Judgment: if g is larger than 1000, go to Step 8; else go to Step 2.
8) Perform data fitting on all X_x and Y_x, respectively.

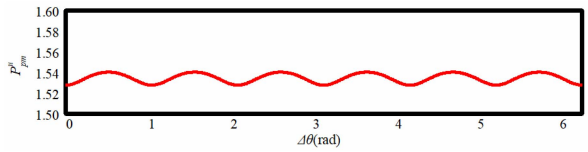

Fig. 4. Optimal standardized maximum phase loss.

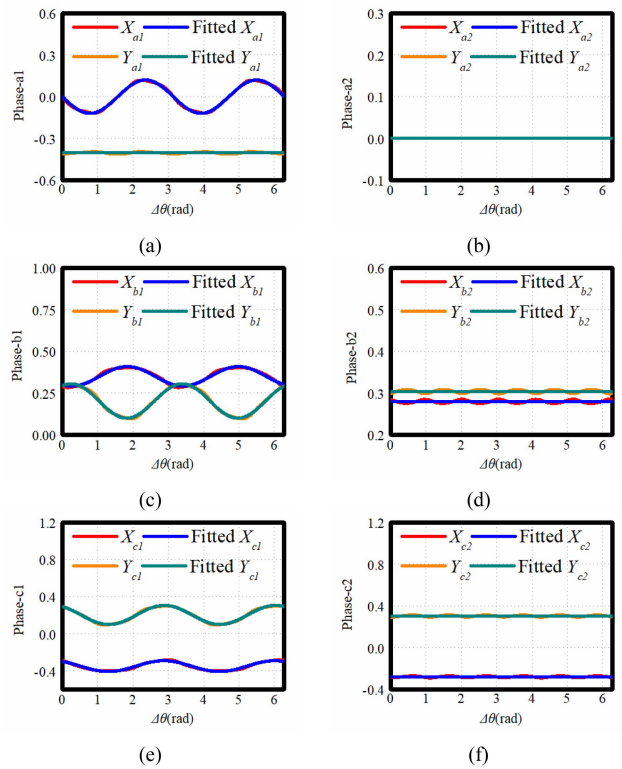

Fig. 5. Fitting results. (a) X_{a1} and Y_{a1}. (b) X_{a2} and Y_{a2}. (c) X_{b1} and Y_{b1}. (d) X_{b2} and Y_{b2}. (e) X_{c1} and Y_{c1}. (f) X_{c2} and Y_{c2}.

By applying above steps, the coefficients (X_x and Y_x) can be deduced by data fitting

$$\begin{cases} X_{a1} = -0.12\sin(2\Delta\theta), Y_{a1} = -0.404 \\ X_{b1} = 0.35 - 0.05\cos(2\Delta\theta) - 0.03\sin(2\Delta\theta) \\ Y_{b1} = 0.202 + 0.09\cos(2\Delta\theta) + 0.05\sin(2\Delta\theta) \\ X_{c1} = -0.35 + 0.05\cos(2\Delta\theta) - 0.03\sin(2\Delta\theta) \\ Y_{c1} = 0.202 + 0.09\cos(2\Delta\theta) - 0.05\sin(2\Delta\theta) \\ X_{a2} = Y_{b2} = 0, X_{b2} = 0.2795, Y_{b2} = 0.3039 \\ X_{c2} = -0.2795, Y_{c2} = 0.3039. \end{cases} \tag{21}$$

Then, the maximum phase loss can be minimized by applying (12) and (21) into (19) and the standardized maximum phase loss can be represented in Fig. 4.

The fitting results are shown in Fig. 5. It can be seen from Fig. 5 that the theoretical value and the fitted value can match well. Hence, the minimized maximum phase loss can be calculated by (21). For the independent-leg fault, the reference $dq0$-axis currents can be deduced by bringing (12) and (21) into (9). Then,

the fault current distributor II can be described as

$$\begin{cases} i_{d1}^{*} = -0.06\mathrm{I}_m \sin\left(2\theta_1 + 2\Delta\theta\right) \\ i_{q1}^{*} = \dfrac{1}{3}\mathrm{I}_m \left[1.21 - 0.18\cos\left(2\theta_1 + 2\Delta\theta\right)\right] \\ i_{01}^{*} = 0.06\mathrm{I}_m \sin\left(\theta_1 - 2\Delta\theta\right) \\ i_{d2}^{*} = 0.06\mathrm{I}_m \sin\left(2\theta_1 + 2\Delta\theta\right) \\ i_{q2}^{*} = \dfrac{1}{3}\mathrm{I}_m \left[0.79 + 0.18\cos\left(2\theta_1 + 2\Delta\theta\right)\right] \\ i_{02}^{*} = 0.2026\mathrm{I}_m \sin\left(\theta_1 + \Delta\theta\right) \end{cases} \tag{22}$$

The $dq0$-axis currents in fault mover with the independent-leg fault satisfy

$$i_{a2} = i_{d2}\cos(\theta_1 + \Delta\theta) - i_{q2}\sin(\theta_1 + \Delta\theta) + i_{02} = 0. \tag{23}$$

Hence, the 0-axis current in fault mover with the independent-leg fault does not need to be controlled if the dq-axis currents have been controlled. However, the $dq0$-axis current constraint (23) does not exist in the common-leg fault. For the common-leg fault, the $dq0$-axis currents need to be controlled separately.

C. Voltage Distributor

In this subsection, the voltage demands are distributed into remaining inverter legs. The voltage distributor mainly includes three conditions: phase without fault; phase with the common-leg fault; and phase with the independent-leg fault.

For different conditions, the voltage demands are deduced as

$$\begin{cases} u_{ay} = u_{ay}^{n} + \Delta u_y \\ u_{by} = u_{by}^{n} + \Delta u_y \\ u_{cy} = u_{cy}^{n} + \Delta u_y \end{cases} \tag{24}$$

where u_{ay}, u_{by}, and u_{cy} are the voltage demands of mover y; Δu_y is the voltage offset of mover y; u_{ay}^{n}, u_{by}^{n}, and u_{cy}^{n} are calculated by inverse Park transformation

$$\begin{bmatrix} u_{ay}^{n} \\ u_{by}^{n} \\ u_{cy}^{n} \end{bmatrix} = \begin{bmatrix} \cos(\theta_y) & -\sin(\theta_y) & 1 \\ \cos(\theta_y - 2\pi/3) & -\sin(\theta_y - 2\pi/3) & 1 \\ \cos(\theta_y + 2\pi/3) & -\sin(\theta_y + 2\pi/3) & 1 \end{bmatrix} \begin{bmatrix} u_{dy} \\ u_{qy} \\ u_{0y} \end{bmatrix} \tag{25}$$

where u_{dy}, u_{qy}, and u_{0y} are the $dq0$-axis voltage of mover y. The superscript n represents the voltage calculated by inverse Park transformation.

For healthy condition and the common-leg fault, the voltage offsets will be zero.

For the independent-leg fault, the current of the fault phase is zero. Hence, the voltage of fault phase is always the back EMF. Then, the fault phase voltage needs to match the inverter voltage. The voltage offsets can be described as

$$\begin{cases} \Delta u_1 = 0 \\ \Delta u_2 = -\omega_e \psi_f \sin(\theta_2) - u_{a2}^{n}. \end{cases} \tag{26}$$

For the phase without fault, the voltage distribution strategy can be described as

$$\begin{cases} \delta_{ap} = \left(2u_{dc} - u_{a1} - u_{a2}\right)/\left(4u_{\mathrm{dc}}\right) \\ \delta_{a1} = \delta_{ap} + \left(u_{a1}/u_{\mathrm{dc}}\right) \\ \delta_{a2} = \delta_{ap} + \left(u_{a2}/u_{\mathrm{dc}}\right) \end{cases} \tag{27}$$

where u_{a1} and u_{a2} are the phase-A voltage.

For the phase with the common-leg fault, the distribution strategy can be described as

$$\begin{cases} \delta_{a1} = \dfrac{u_{a1} - u_{a2}}{2u_{\mathrm{dc}}} + \dfrac{1}{2} \\ \delta_{a2} = \dfrac{u_{a2} - u_{a1}}{2u_{dc}} + \dfrac{1}{2}. \end{cases} \tag{28}$$

For the phase with the independent-leg fault, the distribution strategy can be described as

$$\begin{cases} \delta_{a1} = \dfrac{u_{a1}}{2u_{dc}} + \dfrac{1}{2} \\ \delta_{ap} = \dfrac{-u_{a1}}{2u_{\mathrm{dc}}} + \dfrac{1}{2}. \end{cases} \tag{29}$$

IV. Conventional Fault-Tolerant Control Method

The conventional fault-tolerant control method is designed from the perspective of single mover, which is similar to the fault tolerance of open-end winding drive system. The conventional method also includes two parts: conventional current distributors and conventional voltage distributor. Other parts of control system are same with the drive system in Fig. 2.

A. Conventional Current Distributor I

In the conventional current distributor, the current distribution is similar to that in the conventional open-end winding system with fault [14]. As a result, each mover can output constant thrust under postfault condition. In addition, the thrusts of two movers are distributed in the principle of equal current amplitude. That is, all remaining phase currents always have same phase current amplitude. The conventional current distributor I is designed for the common-leg fault.

For the common-leg fault, all phase currents can be distributed as

$$\begin{cases} i_{a1} = 0, & i_{a2} = 0 \\ i_{b1} = -\mu_1 I_m \sin(\theta_1 - 5\pi/6), & i_{b2} = -\mu_1 I_m \sin(\theta_2 - 5\pi/6) \\ i_{c1} = -\mu_1 I_m \sin(\theta_1 + 5\pi/6), & i_{c2} = -\mu_1 I_m \sin(\theta_2 + 5\pi/6) \end{cases} \tag{30}$$

where μ_1 is the amplitude coefficient for the common-leg fault. Taking (11) and (30) into (2), the value of μ_1 is $\sqrt{3}/3$. The conventional current distributor II can be deduced by bringing (30) into (9)

$$\begin{cases} i_{d1}^{*} = 0, i_{q1}^{*} = I_m/3, i_{01}^{*} = (I_m/3)\sin(\theta_1) \\ i_{d2}^{*} = 0, i_{q2}^{*} = I_m/3, i_{02}^{*} = (I_m/3)\sin(\theta_1 + \Delta\theta). \end{cases} \tag{31}$$

B. Conventional Current Distributor II

The conventional current distributor II is designed for the independent-leg fault. The design is based on the equal current amplitude principle.

For the independent-leg fault, all phase currents can be distributed as

$$\begin{cases} i_{a1} = \mu_2 I_m \sin(\theta_1), & i_{a2} = 0 \\ i_{b1} = \mu_2 I_m \sin(\theta_1 - 2\pi/3), & i_{b2} = -\mu_2 I_m \sin(\theta_2 - 5\pi/6) \\ i_{c1} = \mu_2 I_m \sin(\theta_1 + 2\pi/3), & i_{c2} = -\mu_2 I_m \sin(\theta_2 + 5\pi/6) \end{cases} \tag{32}$$

where μ_2 is the amplitude coefficient for the independent-leg fault. Taking (11) and (32) into (2), the value of μ_2 is $2\sqrt{3}/[3(1+\sqrt{3})]$. The conventional current distributor can be deduced by bringing (32) into (9)

$$\begin{cases} i_{d1}^* = 0, \quad i_{q1}^* = \dfrac{2\sqrt{3}}{3(1+\sqrt{3})} I_m, \quad i_{01}^* = 0 \\ i_{d2}^* = 0, i_{q2}^* = \dfrac{2}{3(1+\sqrt{3})} I_m, i_{02}^* = \dfrac{2}{3(1+\sqrt{3})} I_m \sin(\theta_1 + \Delta\theta) \end{cases} \tag{33}$$

C. Conventional Voltage Distributor

The conventional voltage distributor is designed from the perspective of single mover. The voltage demands of each mover can be calculated by (24). For healthy mover, Δu_y is 0. For fault mover, Δu_y is $-\omega_e \psi_f \sin(\theta_y) - u_{ay}^n$.

For the phase without fault, the duty ratios are distributed by (25). For the phase with the independent-leg fault, the duty ratios are distributed by (26). For the phase with the common-leg fault, the duty ratios are zero.

V. Performance Analysis

In this section, the system copper loss and the thrust output capacity of different fault-tolerant control methods are compared and the system stability is analyzed.

A. Comparison of Different Methods

In this subsection, the proposed method is compared with the conventional method, including the system copper loss and the thrust output capacity.

The system copper loss P_t can be defined based on the (16) as

$$\begin{cases} P_t = P_{a1} + P_{b1} + P_{c1} + P_{a2} + P_{b2} + P_{c2} \\ P_t^u = P_{a1}^u + P_{b1}^u + P_{c1}^u + P_{a2}^u + P_{b2}^u + P_{c2}^u. \end{cases} \tag{34}$$

To compare with the system copper loss, the system copper loss coefficient k_L is defined as

$$k_{\mathrm{L}} = \frac{P_t}{6 \times 0.5 R_x I_h^2} = \frac{P_t^u}{6}. \tag{35}$$

Under healthy condition, when the phase current reach to the rated current I_{rated}, the maximum thrust capacity is F_{rated}, which satisfy (18). Under fault condition, the maximum thrust $F^f{}_{\max}$ can be deduced when the maximum phase copper loss is $0.5 R_x I_{\mathrm{rated}}^2$. Based on the (19), the maximum phase copper loss satisfies

$$P_{\mathrm{pm}}^u \times 0.5 R_x I_{h\_\max}^2 = 0.5 R_x I_{\mathrm{rated}}^2. \tag{36}$$

Then, the maximum equivalent thrust current $I_{\mathrm{h\_max}}$ can be calculated as

$$I_{h\_\max} = I_{\mathrm{rated}} / \sqrt{P_{\mathrm{pm}}^u}. \tag{37}$$

To compare the thrust output capacity, the thrust coefficient k_T is defined as

$$k_T = F_{\max}^f / F_{\mathrm{rated}} = I_{h\_\max} / I_{\mathrm{rated}} = 1 / \sqrt{P_{\mathrm{pm}}^u}. \tag{38}$$

The system copper loss and thrust output capacity of the independent-leg fault are compared in Fig. 6. Compared with the conventional method, the proposed method can increase the thrust output capacity by 2.1%–2.5% and decrease the system copper loss by 4.1%–4.9%. The system copper loss and thrust output capacity of the common-leg fault are compared in Fig. 7. Compared with the conventional method, the proposed method can increase the thrust output capacity by 0%–73.1% and decrease the system copper loss by 13.4%–50%. To conclude, the proposed tolerant method can reduce the system copper loss and increase the thrust output capacity for both independent-leg fault and common-leg fault.

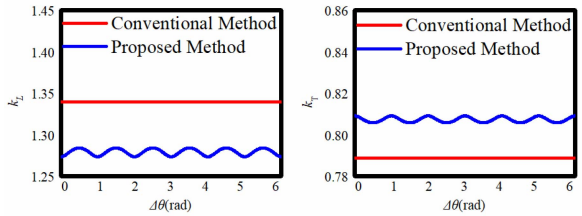

Fig. 6. System copper loss and thrust output capacity of the independent-leg fault. (a) System copper loss coefficient. (b) Thrust coefficient.

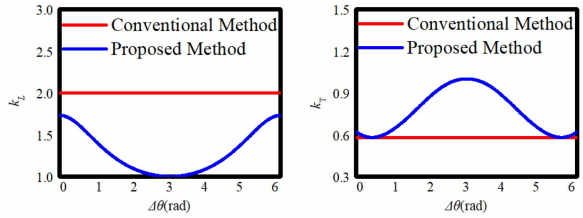

Fig. 7. System copper loss and thrust output capacity of the common-leg fault. (a) System copper loss coefficient. (b) Thrust coefficient.

B. Stability Analysis

In the proposed method, the proportional–integral (PI) controller is adopted in the current regulator. The VSI modulation is equivalent to first-order inertial element. After eliminating decoupling terms, the signal graph of current loop is shown in Fig. 8.

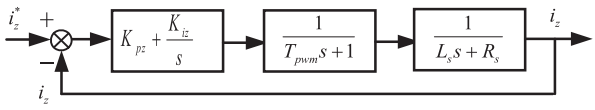

Fig. 8. Signal graph of single current loop.

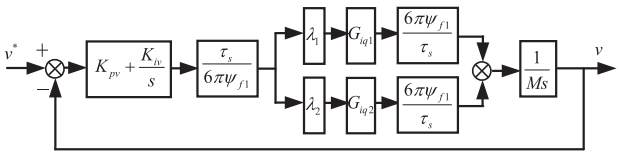

Fig. 9. Signal graph of speed loop.

In Fig. 8, K_{pz} and K_{iz} are PI coefficient of current regulator; $T_{\rm pwm}$ is the switching period; $L_{\rm s}$ is synchronous inductance; and the subscripts z indicates different axis ($z = d1$, $q1$, 01, $d2$, $q2$, 02). By setting $K_{pz} = L_{\rm s}/(2T_{\rm pwm})$ and $K_{iz} = R_{\rm s}/(2T_{\rm pwm})$, the current loop can be corrected to a typical I-order system. The closed-loop transfer function $G_{\rm iz}$ can be deduced as

$$G_{iz} = \frac{1}{2T_{\rm pwm}^2 s^2 + 2T_{\rm pwm}s + 1}. \tag{39}$$

Usually, $T_{\rm pwm}$ is far less than 1. Hence, $G_{\rm iz}$ can be simplified as

$$G_{iz} = \frac{1}{2T_{\rm pwm}^2 s^2 + 2T_{\rm pwm}s + 1} \approx \frac{1}{2T_{\rm pwm}s + 1}. \tag{40}$$

In the system, two movers have the same parameters and same current loop. For the studied mover, the ratio of the third harmonic flux linkage to the fundamental flux linkage is 0.5%. Hence, the influence of zero sequence current on the thrust can be ignored in traction system. Then, the signal graph of speed loop is shown in Fig. 9. In Fig. 9, K_{pv} and K_{iv} are PI coefficient of speed regulator; M is the total mass of two movers; and λ_1 and λ_2 are the ratio of single mover thrust to system thrust. By setting $K_{pv} = (3M)/[10(\lambda_1+\lambda_2)T_{\rm pwm}]$ and $K_{iv} = (3M)/[100(\lambda_1+\lambda_2)T^2_{\rm pwm}]$, the speed loop can be corrected to a typical II-order system. The closed-loop transfer function of speed loop G_v can be deduced as

$$G_v = \frac{3(10T_{\rm pwm}s + 1)}{200T_{\rm pwm}^3 s^3 + 100T_{\rm pwm}^2 s^2 + 30T_{\rm pwm}s + 3}. \tag{41}$$

The pole-zero map of the speed loop transfer function G_v is shown in Fig. 10. When the switching period $T_{\rm pwm}$ change from 0.001 to 0.0005 s, the poles change along three arrows. According to Fig. 10, the poles are always in negative plane and the control system will be always stable. For healthy condition, independent-leg fault condition and common-leg fault condition, the current distributor only affect the value of λ_1 and λ_2. However, λ_1 and λ_2 do not appear in (41). Hence, the system will always remain stable when switching from healthy current distributor to (10) or (22).

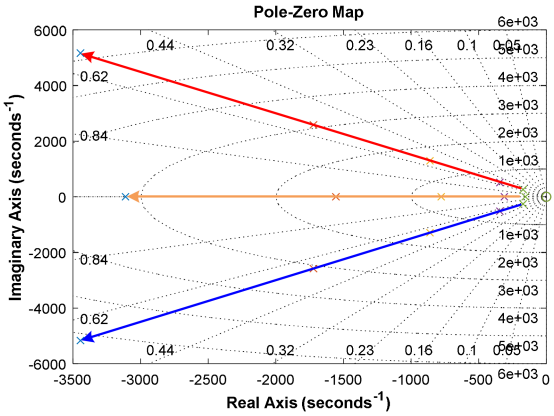

Fig. 10. Pole-zero map of the speed loop transfer function.

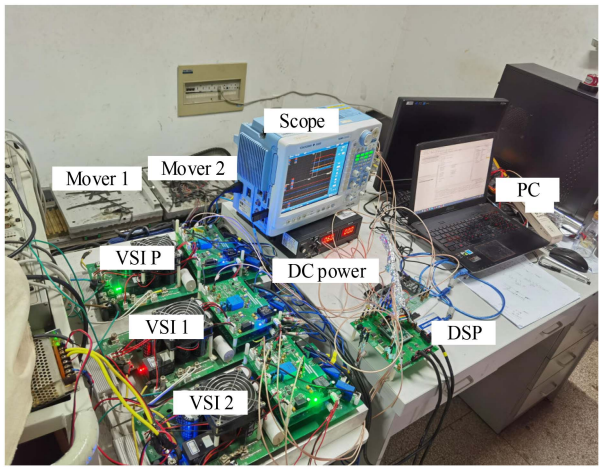

Fig. 11. Experimental setup.

TABLE I
PARAMETERS OF PPMLM

Parameter	Value
Stator resistance (Ω) R_s	3
d-axis inductance (H) $L_{\rm d}$	33.5e-3
q-axis inductance (H) $L_{\rm q}$	33.5e-3
Magnets flux(Wb) $\psi_{\rm f}$	0.125
Double pole pitch (m) $\tau_{\rm s}$	0.024

VI. EXPERIMENTAL VALIDATION

In order to verify the effectiveness of the proposed method, an HCOW experimental setup is developed, as shown in Fig. 11. The setup consists of two linear movers, three VSIs, a DSP control board, a scope, and a dc power source. Two movers have same parameters as listed in Table I. The switching frequency is 10 kHz. The performances of the proposed method are carried out in Experiment 1. The proposed method is compared with the conventional method in Experiment 2.

A. Experiment 1: Verification of the Proposed Method

In this experiment, the proposed method is, respectively, verified in the independent-leg fault and the common-leg fault.

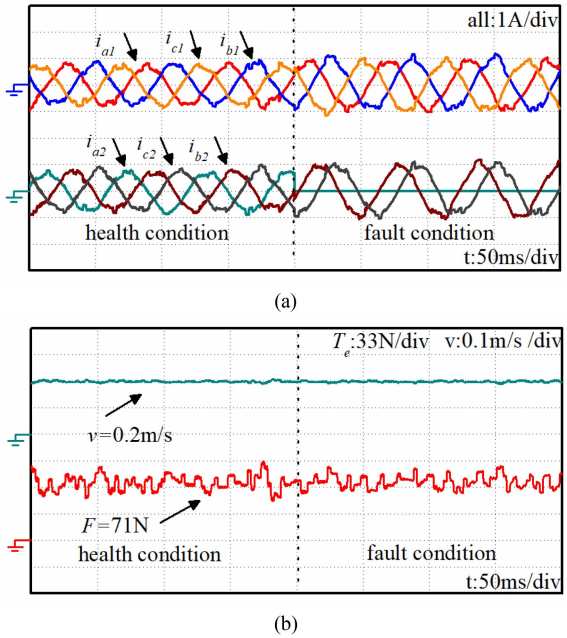

Fig. 12. Experimental results of the proposed method for the independent-leg fault. (a) Phase current. (b) Speed and thrust.

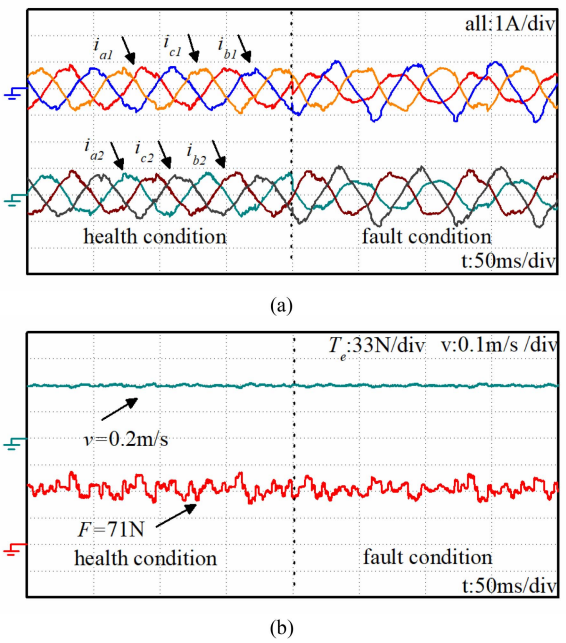

Fig. 13. Experimental results of the proposed method for the common-leg fault. (a) Phase current. (b) Speed and thrust.

The primary position difference $\Delta\theta$ of two movers is $\pi/2$. In Fig. 12, the studied drive system is switched from the healthy condition to the independent-leg fault condition. The thrust and speed have little change before and after fault. In Fig. 13, the studied drive system is switched from the healthy condition to the common-leg fault condition. After fault, the currents of fault phase are completely opposite, which is consistent with the Lagrange loss minimization principle. The thrust and speed also

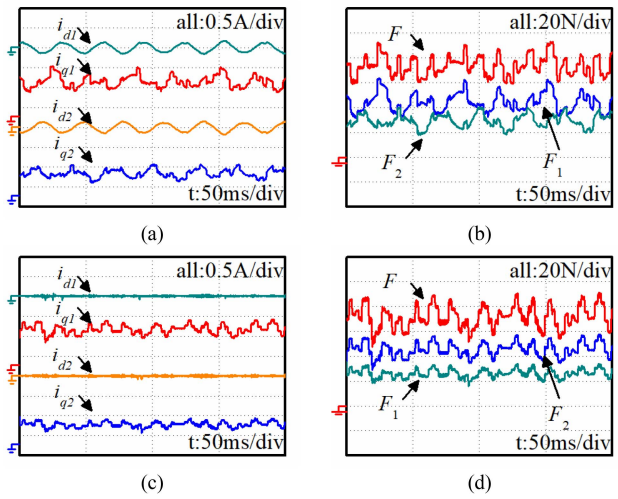

Fig. 14. Experimental results of the proposed method for the independent-leg fault. (a) *dq*-axis current of proposed method. (b) Thrust of proposed method. (c) *dq*-axis current of conventional method. (d) Thrust of conventional method.

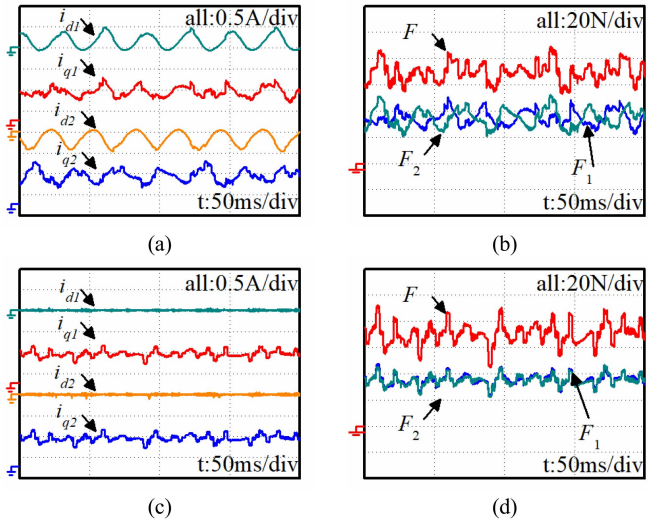

Fig. 15. Experimental results of the proposed method for the common-leg fault. (a) *dq*-axis current of proposed method. (b) Thrust of proposed method. (c) *dq*-axis current of conventional method. (d) Thrust of conventional method.

hardly change. The harmonics in phase current mainly result from the load disturbances, which consist of the uneven track friction, the cogging force, and the ending force. To ensure the stable speed, the thrust should match the load disturbances. This will bring harmonic component to the phase current.

B. Experiment 2: Comparison

In this experiment, the proposed method is compared with the conventional method. The experimental results of the independent-leg fault are shown in Fig. 14. It can be found that both methods have same thrust ripple, while the *dq*-axis currents are different. The experimental results of the independent-leg fault are shown in Fig. 15.

Similarly, both methods also show same thrust output performance. The system copper loss and thrust capacity of the

TABLE II
LOSS COMPARISON FOR THE INDEPENDENT-LEG FAULT

Loss type	Method	$\Delta\theta$ 0	$\pi/4$	$\pi/2$	$3\pi/4$	π
k_T	Proposed	0.798	0.799	0.803	0.799	0.798
	Conventional	0.784	0.784	0.784	0.784	0.784
	Reduction	1.8%	1.9 %	2.4%	1.9%	1.8%
k_L	Proposed	1.260	1.256	1.256	1.253	1.260
	Conventional	1.320	1.322	1.318	1.323	1.321
	Reduction	4.6%	5.0%	4.7%	5.3%	4.6%

TABLE III
LOSS COMPARISON FOR THE COMMON-LEG FAULT

Loss type	Method	$\Delta\theta$ 0	$\pi/4$	$\pi/2$	$3\pi/4$	π
k_T	Proposed	0.620	0.600	0.745	0.924	0.997
	Conventional	0.574	0.574	0.574	0.574	0.574
	Reduction	8.0%	4.3%	30.0%	61.0%	73.7%
k_L	Proposed	1.677	1.481	1.119	1.023	0.972
	Conventional	1.951	1.958	1.946	1.938	1.950
	Reduction	14.0%	24.4%	38.8%	47.2%	50.1%

proposed method are compared with that of the conventional method, as shown in Tables II and III. In Table II, the system copper loss can be decreased and the thrust output capacity can be increased by applying the proposed method to the independent-leg fault. Due to the uneven friction, the reduction of k_T is a little less than theoretical analysis. In Table III, the system copper loss can be decreased and the thrust output capacity can be increased by applying the proposed method to the common-leg fault. In general, the experimental results of the proposed method are consistent with the theoretical analysis.

VII. CONCLUSION

This article proposes a fault-tolerant control method for HCOW motor drive system with OCF. The proposed method can be applied to the common-leg fault and the independent-leg fault. The proposed fault control method includes two fault current distributors and one voltage distributor. The fault current distributor I is applied for the common-leg fault and the fault current distributor II is applied for the independent-leg fault. The voltage distributor is designed to distribute the voltage demand into remaining inverter legs. The voltage distributor includes three conditions: phase without fault; phase with the common-leg fault; and phase with the independent-leg fault. The conventional fault-tolerant control method is designed from the perspective of single mover, which is similar to the fault tolerance of open-end winding drive system. Compared with the conventional method, the system copper loss and phase copper loss of the proposed method can be reduced simultaneously. For the independent-leg fault, the thrust output capacity is increased by 2.1%–2.5% and the system copper loss is decreased by 4.1%–4.9%. For the common-leg fault, the thrust output capacity is increased by 0%–73.1% and the system copper loss is decreased by 13.4%–50%. Finally, the effectiveness of the proposed fault-tolerant control method has been verified by experimental results.

REFERENCES

[1] Z. Song, C. Liu, Z. Dong, and R. Huang, "Improved multi-stage decoupling space vector modulation for asymmetrical multi-phase PMSM with series winding connection," *IEEE Trans. Power Electron.*, vol. 37, no. 9, pp. 10951–10966, Sep. 2022.

[2] Z. Novak and M. Novak, "Adaptive PLL-based sensorless control for improved dynamics of high-speed PMSM," *IEEE Trans. Power Electron.*, vol. 37, no. 9, pp. 10154–10165, Sep. 2022.

[3] W. Wang, W. Tian, Z. Lu, Z. Wang, W. Hua, and M. Cheng, "Fault-tolerant predictive control for five-leg dual-mover permanent-magnet motor drives," *IEEE Trans. Power Electron.*, vol. 38, no. 5, pp. 5803–5815, May 2023.

[4] Y. Du, J. Ji, W. Zhao, T. Tao, and D. Xu, "Self-adapted model predictive current control for five-phase open-end winding PMSM with reduced switching loss," *IEEE Trans. Power Electron.*, vol. 37, no. 9, pp. 11007–11018, Sep. 2022.

[5] S. G. Petkar and V. K. Thippiripati, "A simplified predictive current control of open-end winding permanent magnet synchronous motor," *IEEE Trans. Power Electron.*, vol. 38, no. 1, pp. 816–826, Jan. 2023.

[6] M. Wang, D. Sun, W. Ke, and H. Nian, "A universal lookup table-based direct torque control for OW-PMSM drives," *IEEE Trans. Power Electron.*, vol. 36, no. 6, pp. 6188–6191, Jun. 2021.

[7] W. Tian, W. Wang, Z. Lu, Z. Wang, W. Hua, and M. Cheng, "Collaborative control for half-centralized open-end winding permanent-magnet linear motor drive systems," *IEEE Trans. Power Electron.*, vol. 37, no. 9, pp. 10399–10411, Sep. 2022.

[8] W. Wang, Y. Jiang, W. Tian, W. Hua, and M. Cheng, "Unified maximum voltage utilization controls for half-centralized open-end winding permanent-magnet motor systems," *IEEE Trans. Power Electron.*, vol. 38, no. 1, pp. 372–384, Jan. 2023.

[9] W. Wang, Y. Jiang, L. Sun, Z. Wang, W. Hua, and M. Cheng, "Phase model predictive voltage control for half-centralized open-end winding permanent-magnet linear motor traction systems," *IEEE Trans. Ind. Electron.*, vol. 69, no. 12, pp. 12201–12212, Dec. 2022.

[10] R. R. Errabelli and P. Mutschler, "Fault-tolerant voltage source inverter for permanent magnet drives," *IEEE Trans. Power Electron.*, vol. 27, no. 2, pp. 500–508, Feb. 2012.

[11] H. Zhou, J. Xu, C. Chen, X. Tian, and G. Liu, "Disturbance-observer-based direct torque control of five-phase permanent magnet motor under open-circuit and short-circuit faults," *IEEE Trans. Ind. Electron.*, vol. 68, no. 12, pp. 11907–11917, Dec. 2021.

[12] K. Yu, Z. Wang, M. Gu, and X. Wang, "Universal control scheme of dual three-phase PMSM drives with single open-phase fault," *IEEE Trans. Power Electron.*, vol. 37, no. 12, pp. 14034–14039, Dec. 2022.

[13] G. Yang, S. Li, H. Hussain, J. Zhang, and J. Yang, "A novel SVPWM fault-tolerant strategy for torque ripple reduction of seven-phase induction machines under single-phase open-circuit fault," *IEEE Trans. Power Electron.*, vol. 38, no. 4, pp. 5217–5229, Apr. 2023.

[14] W. Chen, D. Sun, M. Wang, and H. Nian, "Modeling and control for open-winding PMSM under open-phase fault based on new coordinate transformations," *IEEE Trans. Power Electron.*, vol. 36, no. 6, pp. 6892–6902, Jun. 2021.

[15] Z. Song, F. Zhou, Y. Yu, R. Zhang, and S. Hu, "Open-phase fault-tolerant predictive control strategy for open-end-winding permanent magnet synchronous machines without postfault controller reconfiguration," *IEEE Trans. Ind. Electron.*, vol. 68, no. 5, pp. 3770–3781, May 2021.

[16] X. Zhang and C. Xu, "Second-time fault-tolerant topology and control strategy for the open-winding PMSM system based on shared bridge arm," *IEEE Trans. Power Electron.*, vol. 35, no. 11, pp. 12181–12193, Nov. 2020.

[17] O. Bethoux, E. Laboure, G. Remy, and E. Berthelot, "Real-time optimal control of a 3-phase PMSM in 2-phase degraded mode," *IEEE Trans. Veh. Technol.*, vol. 66, no. 3, pp. 2044–2052, Mar. 2017.

[18] X. Zhou, J. Sun, H. Li, M. Lu, and F. Zeng, "PMSM open-phase fault-tolerant control strategy based on four-leg inverter," *IEEE Trans. Power Electron.*, vol. 35, no. 3, pp. 2799–2808, Mar. 2020.

[19] X. Zhou, J. Sun, H. Li, and X. Song, "High performance three-phase PMSM open-phase fault-tolerant method based on reference frame transformation," *IEEE Trans. Ind. Electron.*, vol. 66, no. 10, pp. 7571–7580, Oct. 2019.

[20] S. Ding, H. Tan, J. Hang, K. Ma, and J. Fan, "Optimized OP-FTC for SPMSM considering copper loss minimization," *IEEE Trans. Energy Convers.*, vol. 37, no. 3, pp. 2138–2146, Sep. 2022.

[21] Y. Guo, L. Wu, X. Huang, Y. Fang, and J. Liu, "Adaptive torque ripple suppression methods of three-phase PMSM during single-phase open-circuit fault-tolerant operation," *IEEE Trans. Ind. Appl.*, vol. 56, no. 5, pp. 4955–4965, Sep./Oct. 2020.
[22] L. Wu, Y. Guo, X. Huang, Y. Fang, and J. Liu, "Harmonic torque suppression methods for single-phase open-circuit fault-tolerant operation of PMSM considering third harmonic BEMF," *IEEE Trans. Power Electron.*, vol. 36, no. 1, pp. 1116–1129, Jan. 2021.
[23] A. Sayed-Ahmed, B. Mirafzal, and N. A. O. Demerdash, "Fault-tolerant technique for Δ-connected AC-motor drives," *IEEE Trans. Energy Convers.*, vol. 26, no. 2, pp. 646–653, Jun. 2011.
[24] V. F. Pires, D. Foito, and J. F. Silva, "Fault-tolerant multilevel topology based on three-phase H-bridge inverters for open-end winding induction motor drives," *IEEE Trans. Energy Convers.*, vol. 32, no. 3, pp. 895–902, Sep. 2017.
[25] X. Jiang, W. Huang, R. Cao, Z. Hao, and W. Jiang, "Electric drive system of dual-winding fault-tolerant permanent-magnet motor for aerospace applications," *IEEE Trans. Ind. Electron.*, vol. 62, no. 12, pp. 7322–7330, Dec. 2015.
[26] X. Jiang, Q. Li, W. Huang, and R. Cao, "A dual-winding fault-tolerant motor drive system based on the redundancy bridge arm," *IEEE Trans. Ind. Electron.*, vol. 66, no. 1, pp. 654–662, Jan. 2019.
[27] J. Zhu, H. Bai, X. Wang, and X. Li, "Current vector control strategy in a dual-winding fault-tolerant permanent magnet motor drive," *IEEE Trans. Energy Convers.*, vol. 33, no. 4, pp. 2191–2199, Dec. 2018.
[28] T.-H. Liu, J.-R. Fu, and T. A. Lipo, "A strategy for improving reliability of field-oriented controlled induction motor drives," *IEEE Trans. Ind. Appl.*, vol. 29, no. 5, pp. 910–918, Sep./Oct. 1993.
[29] W. Tian, W. Wang, W. Hua, and M. Cheng, "A general control method for half-centralized open winding permanent-magnet motor drive system," *IEEE Trans. Ind. Electron.*, to be published, doi: 10.1109/TIE.2023.3265038.

Weijie Tian was born in Jiangsu Province, China. He received the B.Sc. degree in electrical engineering from the Shenyang University of Technology, Shenyang, China, in 2018. He is currently working toward the Ph.D. degree in electrical engineering with the Southeast University, Nanjing, China.

His research interests include fault diagnosis and control of electrical machine drive systems.

Wei Wang (Senior Member, IEEE) was born in Jiangsu, China. He received the B.Sc. degree in electrical engineering from the Nanjing University of Science & Technology, Nanjing, China, in 2008, and the Ph.D. degree in electrical engineering from the Southeast University, Nanjing, China, in 2014.

Since 2014, he has been with the Southeast University, where he is currently an Associate Professor with the School of Electrical Engineering. From 2011 to 2012, he got the scholarship from the China Scholarship Council and was a joint Ph.D. student with the University of Lille 1, Lille, France. He has authored or coauthored more than 80 technical papers. His research interests include motor drives, fault-tolerant control, and servo control.

Wei Hua (Senior Member, IEEE) was born in Taizhou, China, in 1978. He received the B.Sc. and Ph.D. degrees in electrical engineering from the Southeast University, Nanjing, China, in 2001 and 2007, respectively.

Since 2007, he has been with the Southeast University, where he is currently a Professor with the School of Electrical Engineering. He has authored or coauthored more than 100 technical papers and holds 44 patents in his areas of interest. His research interests include the design, analysis, and control of electrical machines.

Ming Cheng (Fellow, IEEE) received the B.Sc. and M.Sc. degrees from the Department of Electrical Engineering, Southeast University, Nanjing, China, in 1982 and 1987, respectively, and the Ph.D. degree from the Department of Electrical and Electronic Engineering, University of Hong Kong, Hong Kong, in 2001, all in electrical engineering.

From January to April 2011, he was a Visiting Professor with the Wisconsin Electric Machine and Power Electronics Consortium, University of Wisconsin, Madison, WI, USA. Since 1987, he has been with Southeast University, where he is currently a Distinguished Professor with the School of Electrical Engineering and the Director of the Research Center for Wind Power Generation. He has authored or coauthored more than 300 technical papers and four books, and is the holder of 70 patents in the areas of his teaching and research interests, which include electrical machines, motor drives for EV, and renewable energy generation.

Dr. Cheng is a Fellow of the Institution of Engineering and Technology. He was the Chair and an Organizing Committee Member for many international conferences. He is a Distinguished Lecturer of the IEEE Industry Applications Society for 2015/2016.